

# Experimental and numerical analysis of in- and out- of plane constraint effects on fracture parameters: Aluminium alloy 2024

S. Seitl<sup>a,\*</sup>, P. Hutař<sup>a</sup>, T. E. García<sup>b</sup>, A. Fernández-Canteli<sup>b</sup>

<sup>a</sup>*Institute of Physics of Materials, Academy of Sciences of the Czech Republic, v. v. i. Žitkova 22, 616 62 Brno, Czech Republic*

<sup>b</sup>*Oviedo University, Dept. of Construction and Manufacturing Engineering; E.P.S. de Ingeniería de Gijón, University of Oviedo, Campus de Viesques, 33203 Gijón, Spain*

Received 10 December 2012; received in revised form 26 June 2013

---

## Abstract

The influence of in- and out- of plane constraints on the behaviour of a crack under mode I loading conditions is studied. The independence of the stress intensity tensor, with respect to the specimen thickness  $B$  shows that under loss of constraint conditions higher order members of the Williams' tensor expansion must be considered if the experimental results for increasing apparent fracture toughness resulting from decreasing specimen thickness are to be explained. This is achieved using the constraint curves that define the intensity field tensor along the crack propagation direction and can be alternative to the T-stress approach. This approach is then applied to crack instability assessment for program compact tension (CT — positive values of T-stress) and three point bending (3PB — from negative to positive values of T-stress) specimens with different thicknesses. The theoretical results are compared with experimental ones obtained from the research program on aluminium alloy 2024.

© 2013 University of West Bohemia. All rights reserved.

*Keywords:* LEFM, stress intensity tensor, constraint, aluminium alloy, plane strain, plane stress

---

## 1. Introduction

The character of the stress fields near the crack front has been extensively studied for years [17]. The classical linear elastic fracture mechanics approach stems from the influence of the singular term of the asymptotic expression, determined by its amplitude, or stress intensity factor (SIF, [8]). More accurate two-parameter approaches such as SIF — T-stress [1] or SIF —  $T_{zz}$  in thin elastic plates [7, 14] have been developed to describe the stress field in the vicinity of the crack tip. Such approaches have been applied successfully in engineering fracture design though they are unable to describe the effect of the out-of-plane constraint on the crack-tip field and the fracture toughness. In fact, it is well known that the fracture toughness highly depends on the thickness of the test specimen, so that considering variable fracture toughness, according to the 3D out-of-plane stress level, is inconceivable in practical engineering applications.

The 3D crack-front fields have been studied by different authors [9, 10, 13], as have the effect of  $T_{zz}$  on the 3D crack front fields and fracture toughness [7], proving their application to fracture and fatigue problems.

In particular, the importance of the stress intensity tensor is acknowledged. The effect of in- and out-of-plane constraint is investigated on the basis of previous analytical and numerical results [3–6, 11, 12] supported by a tensor approach based on the Williams' tensor expansion [17]. Apparently, increasing fracture toughness resulting from decreasing specimen thickness can be

---

\*Corresponding author. Tel.: +420 532 290 361, e-mail: seitl@ipm.cz.

explained. The main aim of this work is to investigate the influence of specimen thicknesses on the values of the fracture mechanical parameters using constraint local fracture mechanics. This approach is then applied to crack instability assessment for program compact tension (CT — positive values of  $T$ -stress) and three point bending (3PB — from negative to positive values of  $T$ -stress) specimens made from aluminium alloy 2024 with different thicknesses to explain the change of Al 2024 fracture toughness values obtained from the experiment.

## 2. Tensor description at the crack front

In the following the general expression of the stress field in the proximity of the crack front is derived using a tensor description particularized for the case of pure mode I (the crack propagates in  $x$  direction,  $\theta_{cr} = 0$ ). It comprises the definition of the following magnitudes related to the stress fields  $\sigma_{ij}(r, \theta, z; B)$  in front of the crack front, see Fig. 1.

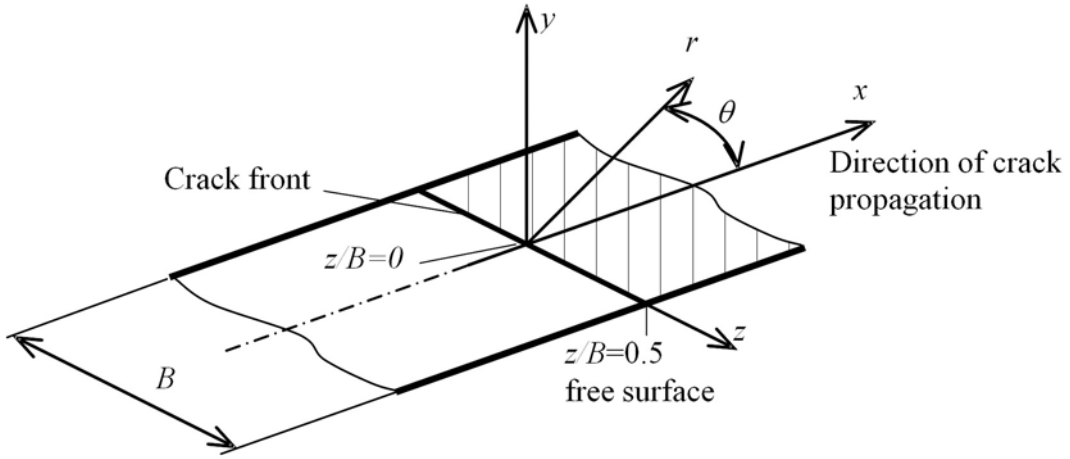


Fig. 1. Crack front and associated coordinate systems (Cartesian and polar)

1. Stress intensity field tensor:

$$\phi_{ij}(r, \theta, z; B) = \sqrt{2\pi r} \sigma_{ij}(r, \theta, z; B). \quad (1)$$

2. Spatial stress intensity tensor:

$$k_{ij}^*(\theta, z; B) = \lim_{r \rightarrow 0} \phi_{ij}(r, \theta, z; B) = \lim_{r \rightarrow 0} \sqrt{2\pi r} \sigma_{ij}(r, \theta, z; B). \quad (2)$$

3. Stress intensity tensor:

$$k_{ij}(z; B) = k_{ij}^*(\theta, z; B)|_{\theta=0} = \lim_{r \rightarrow 0} \sqrt{2\pi r} \sigma_{ij}(r, \theta, z; B)|_{\theta=0}. \quad (3)$$

4. Spatial constraint tensor, defined as that corresponding to the second term of the Williams' expansion:

$$t_{ij}^*(\theta, z; B) = \lim_{r \rightarrow 0} \sqrt{2\pi r} \sigma_{ij}(r, \theta, z; B) - \frac{k_{ij}^*}{\sqrt{2\pi r}}. \quad (4)$$

5. Constraint tensor:

$$t_{ij}(z; B) = t_{ij}^*(\theta, z; B)|_{\theta=0} = \lim_{r \rightarrow 0} \left[ \sigma_{ij}(r, \theta, z; B) - \frac{k_{ij}^*}{\sqrt{2\pi r}} \right] |_{\theta=0}. \quad (5)$$

6. Constraint function:

$$\psi_{ij}(r, \theta, z; B) = \frac{k_{ij}^*(\theta, z; B)}{\sqrt{2\pi}} r^{-1/2} + t_{ij}^*(\theta, z; B) r^0 + O_{ij}(r, \theta, z; B). \quad (6)$$

Using the equations (2) and (4), the stress tensor  $\sigma_{ij}$  in the proximity of a straight crack tip in a plane normal to the crack front at the point  $(r, \theta, z; B)$  for a given specimen thickness  $B$ , see Fig. 1, can be expressed in polar coordinates as the Williams' expansion:

$$\sigma_{ij}(r, \theta, z; B) = \frac{k_{ij}^*(\theta, z; B)}{\sqrt{2\pi}} r^{-1/2} + t_{ij}^*(\theta, z; B) r^0 + O_{ij}(r^{1/2}, \theta, z; B), \quad (7)$$

where  $O_{ij}$  represents the remaining higher order terms as a function of the polar coordinates  $r, \theta, z$  and the thickness  $B$ .

For the Cartesian system in Fig. 1, the stress intensity tensor  $k_{ij}$  for a specimen of the thickness  $B$  at the mid-plane under mode I loading ( $\theta_{cr} = 0$ ) is invariably given by:

$$k_{ij}(z; B) = \begin{pmatrix} K_I(z; B) & 0 & 0 \\ 0 & K_I(z; B) & 0 \\ 0 & 0 & 2\nu K_I(z; B) \end{pmatrix} = K_I(z; B) \begin{pmatrix} 1 & 0 & 0 \\ 0 & 1 & 0 \\ 0 & 0 & 2\nu \end{pmatrix}. \quad (8)$$

The tensor  $t_{ij}$  for a specimen of the thickness  $B$  in the proximity of the crack front, not close to the crack edge, under mode I loading ( $\theta_{cr} = 0$ ) is given by

$$t_{ij}(z; B) = \begin{pmatrix} t_{xx}(z; B) & 0 & 0 \\ 0 & 0 & 0 \\ 0 & 0 & t_{zz}(z; B) \end{pmatrix} = \begin{pmatrix} T(z; B) & 0 & 0 \\ 0 & 0 & 0 \\ 0 & 0 & E\varepsilon_{zz}(z; B) + \nu T(z; B) \end{pmatrix}. \quad (9)$$

By identifying (8)–(9) with the conventional formulation of the Williams' expansion for the case of mode I,  $k_{ij}^*$  can be expressed in terms of  $K_I$  and  $t_{ij}$  can be expressed in term of T-stress:

$$\begin{aligned} k_{ij}(\theta, z; B) &= K_I(z; B) f_{ij}^{(K)}(\theta), \\ t_{ij}(\theta, z; B) &= T(z; B) f_{ij}^{(T)}(\theta), \end{aligned} \quad (10)$$

where  $K_I$  is the stress intensity factor for mode I and  $T$  is the classical  $T$ -stress and  $f_{ij}(\theta)$  are geometric functions with super index ( $T$ ) or ( $K$ ) referred, respectively. See more in [3–6].

### 3. Experimental program and its results

In order to verify the suitability of the tensor description of the stress field, an experimental program was launched.

### 3.1. Specimens and methods

For this purpose, three point bending (3PB, see schematic diagram in Fig. 5) and compact tension (CT, see schematic diagram in Fig. 6) specimens made of aluminium alloy 2024 with different thicknesses ( $B = 5$  mm and 20 mm) and different crack length ratios  $a/W \in (0.2; 0.7)$  were tested (more than 30 specimens). The specimen width was  $W = 50$  mm in all cases. The material parameter  $K_{IC}$  (fracture toughness) was determined according to the British standard method [2] and ASTM E1820 [15].

First, the specimens were notched in different notch lengths and thereafter they were cyclically loaded until approximately 5 mm pre-crack was achieved. After the test the total crack length was measured and the corresponding ratio  $a/W$  was calculated. The crack surface of the fractured specimens is shown in Fig. 2. There are three parts of the surface: i) notch surface, ii) fatigue pre-crack surface and iii) brittle surface. The left and right parts of Fig. 2 show the typical specimen surfaces after the measurement for  $B = 20$  mm and 5 mm, respectively.

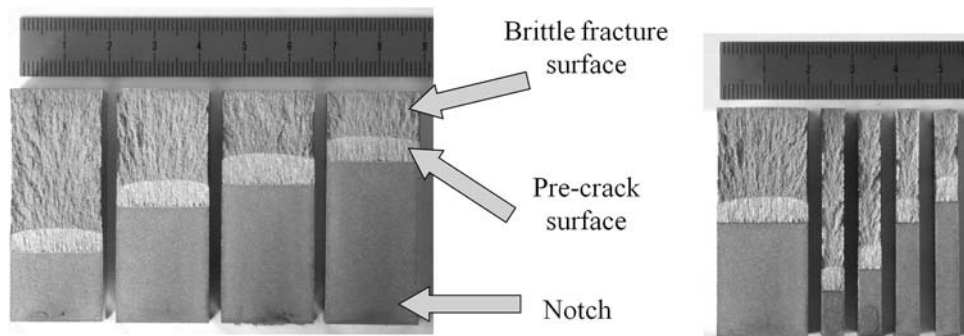


Fig. 2. Crack surfaces of specimens for various ratios  $a/W$  after failure for thicknesses  $B = 20$  mm (left) and 5 mm (right)

### 3.2. Experimental results

For the used material Al 2024, the experimental results are indicated below. The obtained results are presented by values of the fracture toughness  $K_{IC}$  (for mode I) that is divided by  $K_{ICnorm}$  (the value for fracture toughness for plane strain condition  $B \rightarrow \infty$ ).

The ratios of fracture toughness for the 3PB and CT specimens (see Figs. 5 and 6, respectively) with various thicknesses  $B$  (5 mm and 20 mm)  $K_{IC}$ , is determined for the various total crack length ratios  $a/W \in (0.2; 0.7)$ , see Figs. 3 and 4.

The experimentally obtained results for 3PB specimen are shown in Fig. 3. The thin specimens ( $B = 5$  mm) provide fracture toughness  $K_{IC}$  values higher in the first part of interval  $a/W \in (0.2; 0.4)$  than those provided by wide specimens ( $B = 20$  mm). The remaining part of both curves  $a/W \in (0.5; 0.8)$  are similar.

The results for CT specimens are shown in Fig. 4. For thin specimens (thickness  $B = 5$  mm), the values of fracture toughness  $K_{IC}$  are higher in the whole interval  $a/W \in (0.2; 0.8)$  than those provided by wide specimens (thickness  $B = 20$  mm).

In the following the experimental results are correlated with constraint characteristics.

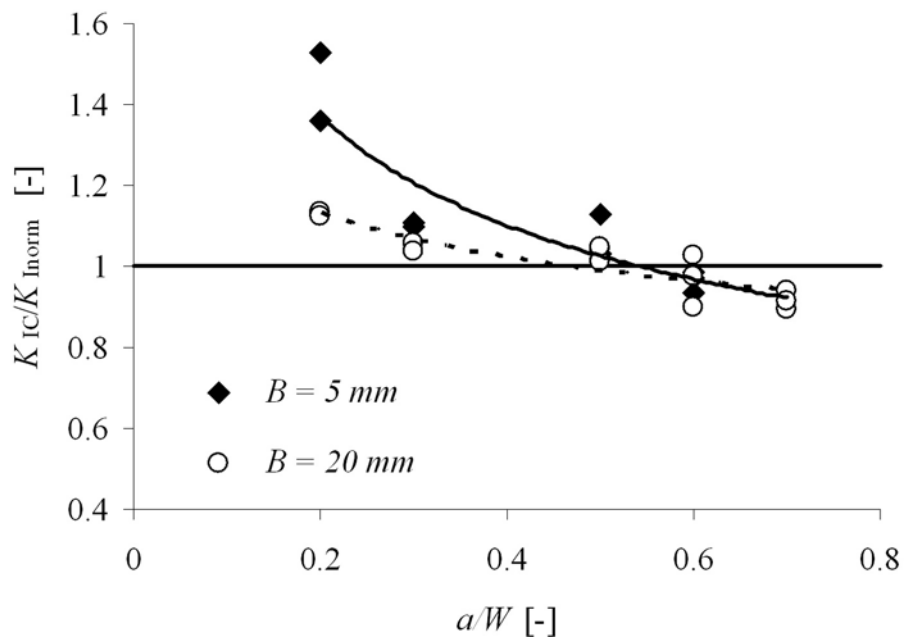


Fig. 3. Dependence of  $K_{IC}/K_{ICnorm}$  with respect to  $a/W$  determined for three point bending specimen

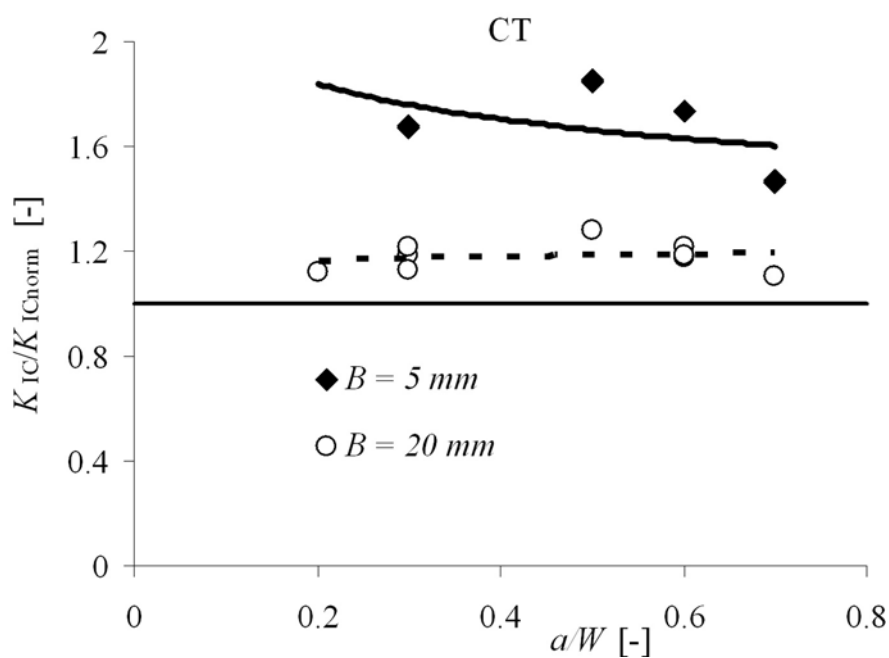


Fig. 4. Dependence of  $K_{IC}/K_{ICnorm}$  with respect to  $a/W$  determined for compact tension specimen

#### 4. Numerical calculation and its results

With the aim of checking the validity of the preceding theoretical derivations and experimental results, linear elastic numerical calculations were performed for material parameters Al 2024 using the finite element code ANSYS.

#### 4.1. Numerical models

The numerical models were in line with the experimental program prepared for two basic geometries: three points bend (3PB) (see Fig. 4) and compact tension (CT) specimens (see Fig. 5) with different crack ratios  $a/W = 0.2; 0.41$  and  $0.7$ . The ratio  $a/W = 0.41$  has been selected because there is for 3PB specimen the value of T-stress equals 0 for 2D solution. The rank of specimen thicknesses were extended about the thickness  $B = 2$  mm to cover theoretically possible slim specimens, so the values of thicknesses  $B = \{2, 5, 20\}$  mm were used for numerical study. The crack ratios  $a/W$  were selected to cover all cases of constraint level for 3PB specimen that is valid for 2D solution ( $T < 0, T = 0, T > 0$ ).

A homogenous linear elastic material model with the Young's modulus  $E = 0.72$  GPa and the Poisson's ratio  $\nu = 0.34$  was taken into account (the material parameters corresponding to AI 2024).

The Fig. 5 shows a schematic diagram of the 3PB model, the used dimensions and its boundary conditions. The Fig. 6 shows schematic diagram of the CT model, the used dimensions and its load.

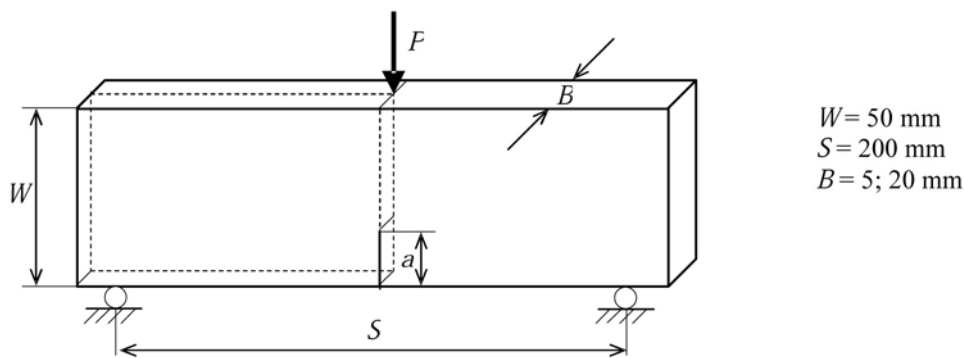


Fig. 5. Schematic diagram of three points bend specimen (3PB)

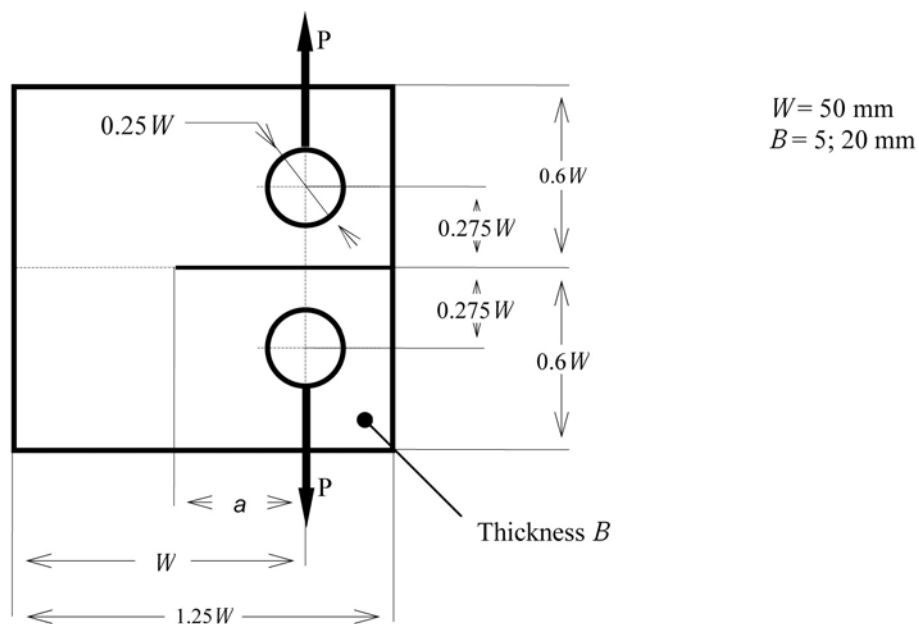


Fig. 6. Schematic diagram of compact tension specimen (CT)

#### 4.2. Numerical results

##### a) Validation of presented model

As the first step, the 2D numerical models presented for the assessment of the fracture mechanics parameters were compared with the data published in [16] for the 2D solution. As the second step, the numerical models were extended to 3D and the Poisson's ratio  $\nu = 0$  was used for the basic validation of this 3D model.

##### b) Numerical results for 3D models

The aim of this work is to find a correlation between the experiment results (see section 3) and the parameters describing the stress field in front of the crack. To that end, in this section 3PB and CT numerical models with various thicknesses are studied. The values of loading  $P$  corresponding to  $K_{ICnorm}$  (the fracture toughness of Al 2024 for plane strain condition  $B \rightarrow \infty$ ) were estimated as functions of the ratio  $a/W$  and were used for  $K_I$  estimation from 3D calibration curves. Theoretically, the same stress fields around the crack tip should be obtained.

As representatives' parameters from the Williams' tensor description curves of  $K_I$ ,  $T_{xx}$ ,  $\varepsilon_{zz}$  and  $T_{zz}$ , were selected; see section 2.

As the first parameters, the stress intensity factors estimated for various specimen thicknesses are shown in Fig. 7. The dependence of  $K_I$  with respect to the thickness  $B$  is dominant

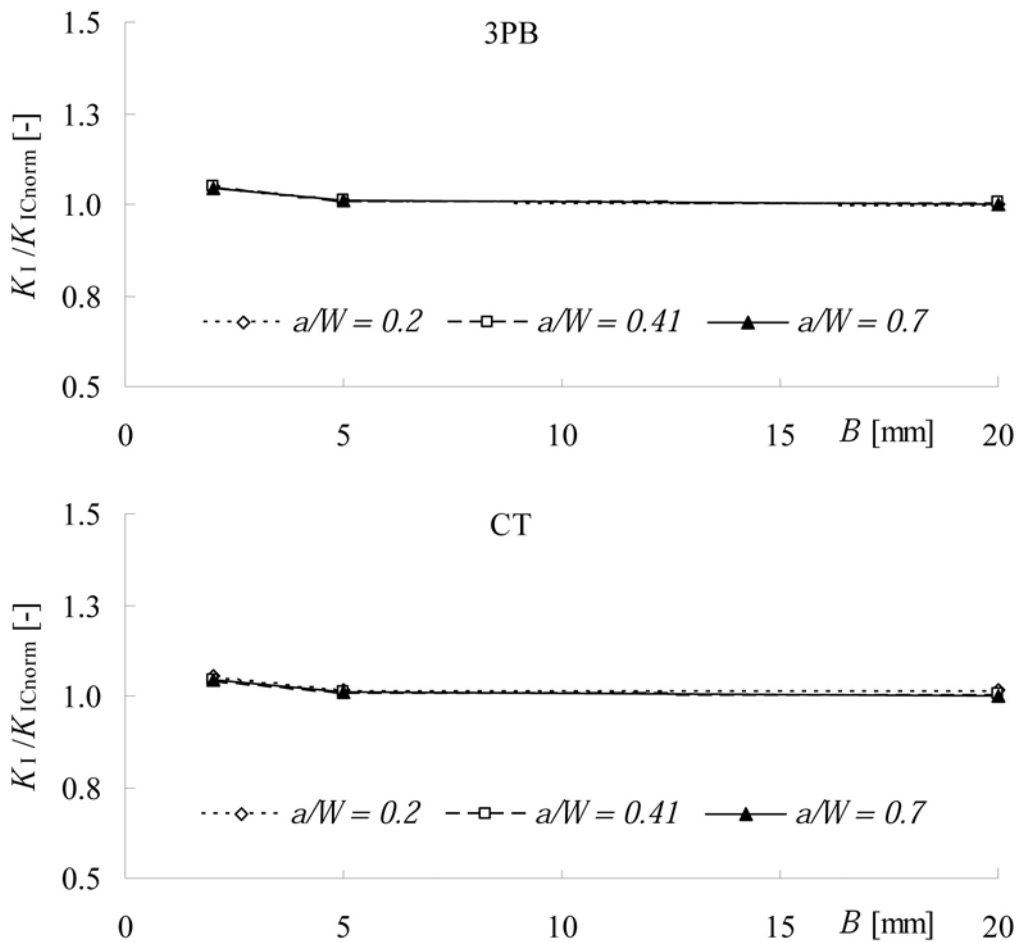


Fig. 7. Change of the values of the stress intensity factors ( $K_I/K_{ICnorm}$ ) along the 3PB and CT specimen's thickness

for the change of values for both cases 3PB and CT specimens. For the infinity thickness, the value will be equal to 1. The influence of the relative crack length ( $a/W$ ) on the values of  $K_I$  is not apparent.

The shapes of the curves of the second parameter, the  $T_{xx}$ -stress, significantly depend on the specimen thickness, as shown in Fig. 8. The value of  $T_{xx}$  grows as the specimen thickness decreases. The difference between the two dimensional (plane strain,  $B \rightarrow \infty$ ) and three dimensional solutions, especially for the thin structures, is essential. According to the results obtained, we can say that the parameter characterizing the constraint ( $T_{xx}$ ) is much more sensitive to the effect of the free surface than the stress intensity factor values and the two dimensional solution of the  $T_{xx}$  can lead to significant discrepancies in comparison with the 3D solution that is more close to reality. Especially for the relative crack length  $a/W = 0.2$  in Fig. 8. For 3PB specimen, according to the 2D solution, there is a negative value of the  $T_{xx}$ , but for the 3D solution the value of  $T_{xx}$  is positive.

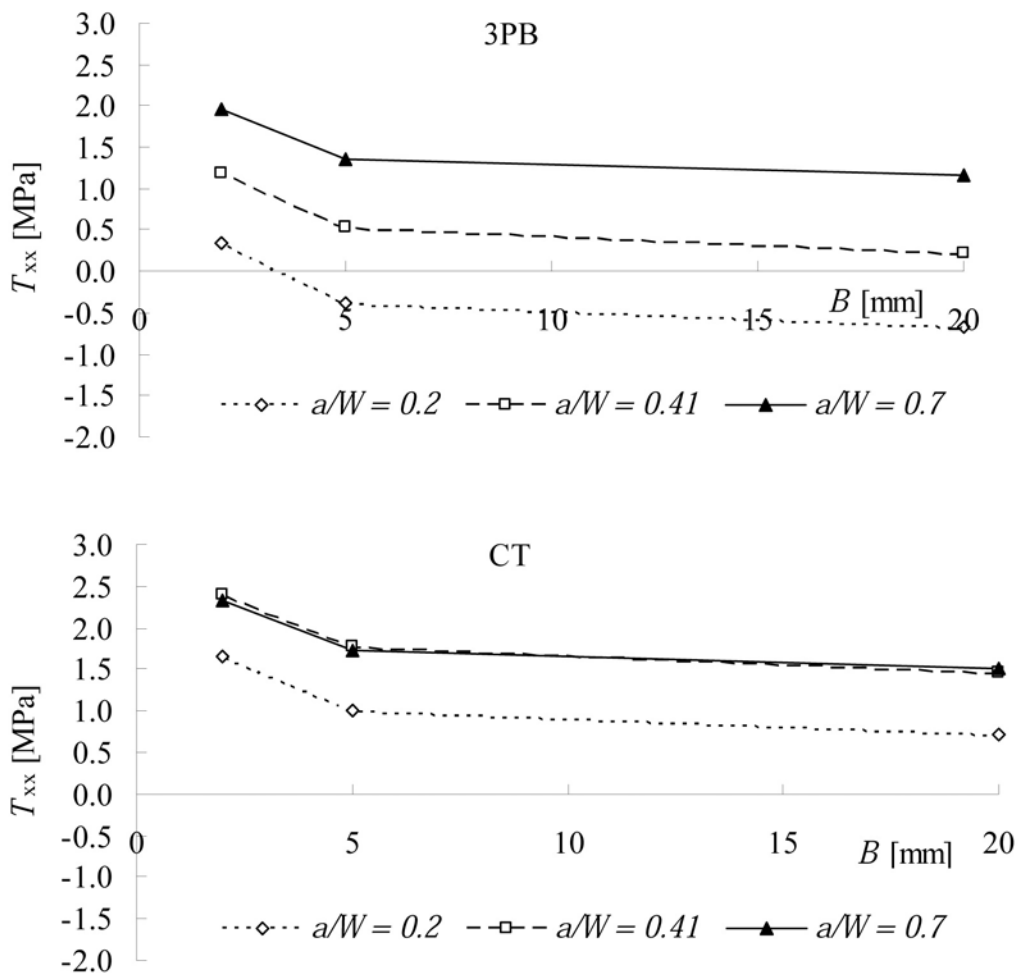


Fig. 8. Change of the values of  $T$ -stress (xx) along the 3PB and CT specimen's thickness

For determining the second parameter  $T_{zz}$  of the Williams' tensor description, the knowledge of the  $\varepsilon_{zz}$  values is required, see eq. (9). The values of out of plane strain  $\varepsilon_{zz}$  are shown in Fig. 9. The curves of  $\varepsilon_{zz}$  are plotted as functions of the specimen thickness  $B$ . The results for the different specimen thicknesses corroborate that the out of plane strain  $\varepsilon_{zz}$  is not zero as

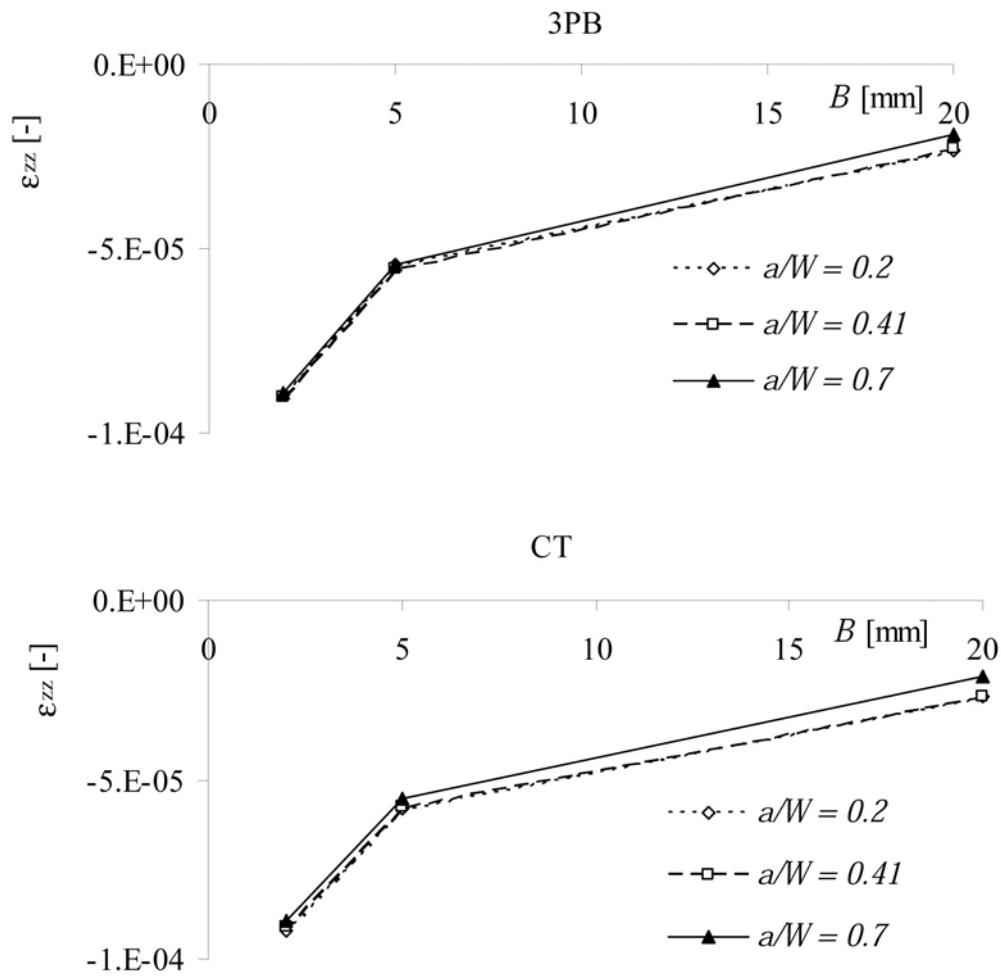


Fig. 9. Change of the values of  $\varepsilon_{zz}$  along the 3PB and CT specimen's thickness

supposed in the 2D solution. The  $\varepsilon_{zz}$  curves tend to zero when the specimen thickness is going to infinity ( $B \rightarrow \infty$ ). The trend of both  $\varepsilon_{zz}$  curves for 3PB and CT specimens is the same due mainly to the influence of the specimen thickness.

As the second parameter of the Williams' tensor description, the change of  $T_{zz}$  is shown in Fig. 9. According to theory the values of  $T_{zz}$  for the thickness  $B \rightarrow \infty$  tends towards zero. For decreasing values of thickness  $B$  the effect of the out of plane constraint increases.

It follows from the performed calculations that the in-plane and the out-of-plane constraint effects mix in 3D cases and that the elastic crack front fields become much more complicated than the 2D one. Two common types of fracture test specimens were examined: 3PB and CT specimens. These specimens represent two typical loading configurations in fracture analyses. To find out the characteristic effects of the specimen thickness, we experimentally tested different thicknesses of both specimen types in the present paper. The trend of the experimental results can be attributed to different level of constraint in both cases.

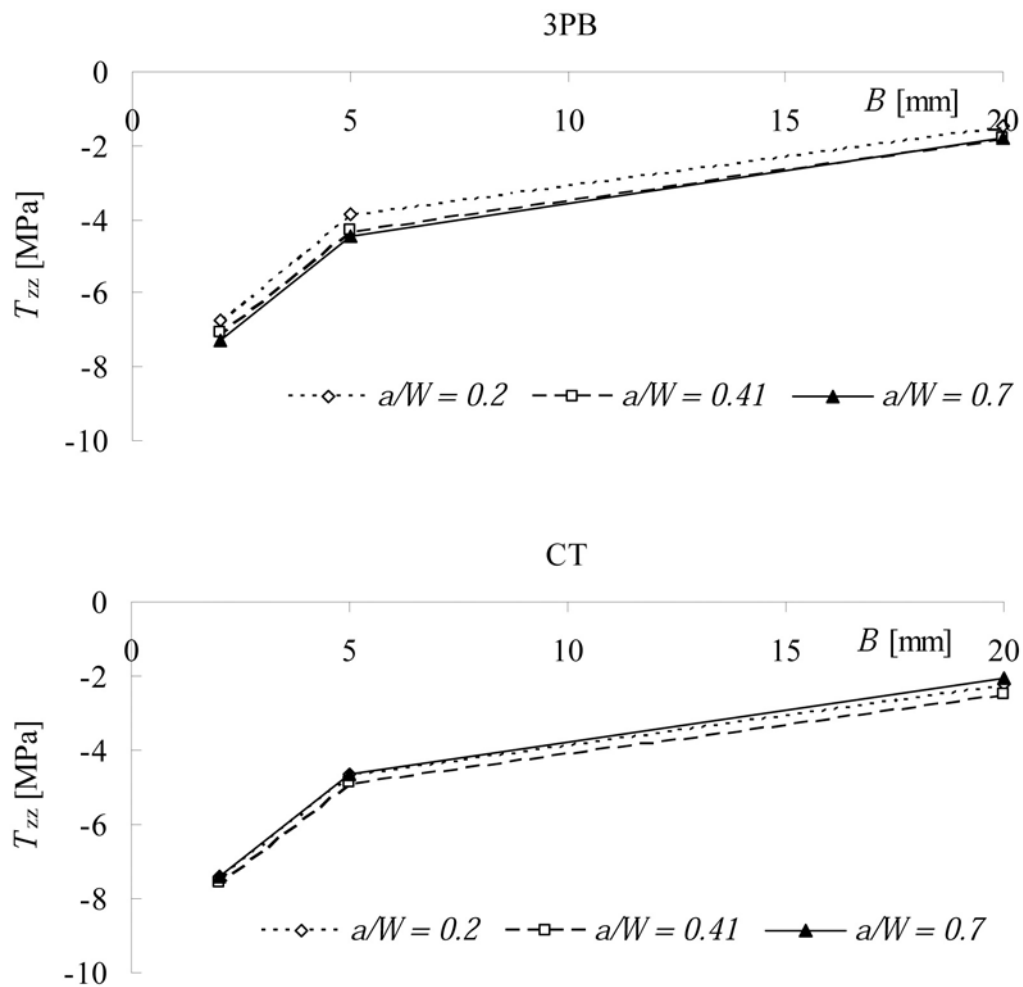


Fig. 10. Change of the values of  $T_{zz}$  along the 3PB and CT specimen's thickness

## 5. Conclusion

The results from the numerical solution and the experimental program are presented. These results were obtained for Al 2024 specimens. Two different geometries (3PB and CT) and two different thicknesses ( $B = 20$  mm and 5 mm) were used. The following conclusions can be made:

- To explain the dependence of  $K_{IC}$  values on specimen thickness, the constraint characteristics (in- and out-of-plane) have to be used.
- Moreover, especially for thin specimens with  $B < 5$  mm, the numerical support for experiment has to be done on the base of a 3D model.
- The experimental results support the analytical derivations found by using the tensor approach.
- The trend of the resulting  $K_{IC}$  curves for different  $a/W$  values can be attributed to simultaneous influence of both  $T_{xx}$  and  $T_{zz}$  stresses.

- Further calculations are envisaged to analyse the stress relations in the state after, particularly in what concerns the constraint evolution during the crack growth process.
- The analytical derivations and the numerical calculations prove the utility of the tensor approach proposed in this work.

## **Acknowledgements**

This work was supported by the Academy of Sciences of the Czech Republic, projects M10041090 and M100411204, and by the Spanish Ministry of Science and Innovation, Project BIA2010-19920.

## **References**

- [1] Betegon, C., Hancock, J., Two parameter characterization of elastic-plastic crack-tip fields, *Journal of Applied Mechanics*, 113 (1991) 104–110.
- [2] British standard method for determination of the rate of fatigue crack growth in metallic materials 1998.
- [3] Fernández-Zúñiga, D., Giner, E., Fernández-Sáez, J., Fernández-Canteli, A., Modelo tensorial para el análisis tridimensional de placas fisuradas solicitadas en modo II y modo mixto, *Anales de Mecánica de la Fractura* 28 (2011) 631–636. (in Spanish)
- [4] Fernández-Canteli, A., Castillo, E., Fernández-Zúñiga, D., Lateral constraint index to assess the influence of specimen thickness, *Proceedings of the 16th European Conference of Fracture*, Alexandropoulis, Greece, 2006, pp. 1–8.
- [5] Fernández-Canteli, A., Giner, E., Fernández-Zúñiga, D., Fernández-Sáez, J., Considerations concerning plane stress and plane strain at the crack front, *Proceedings of the XIII Portuguese Conference on Fracture*, Porto, Portugal, 2012, pp. 1–6.
- [6] Fernández-Canteli, A., Giner, E., Fernández-Zúñiga, D., Fernández-Sáez, J., A unified analysis of the in-plane and out-of-plane constraints in 3-D linear elastic fracture mechanics, *Proceedings of the 19th European Conference on Fracture*, Kazan, Russia, 2012, pp. 1–8.
- [7] Guo, W., Recent advances in three-dimensional fracture mechanics, *Key Engineering Materials* 183 (2000) 193–198.
- [8] Irwin, G. R., *Fracture*, Handbuch der Physik 6. Springer-Verlag, Heidelberg (1958) 551–590.
- [9] Kwon, S. W., Sun, C. T., Characteristics of three-dimensional stress fields in plates with a through the thickness crack, *International Journal of Fracture* 104 (2000) 291–315.
- [10] Nakamura, T., Parks, D. M., Three-dimensional stress field near the crack front of a thin elastic plate, *Journal of Applied Mechanics* 55 (1988) 805–813.
- [11] Seitzl, S., Fernández-Zúñiga, D., Fernández-Canteli, A., Using a tensor model for analyzing some aspects of mode-II loading, *Applied and Computational Mechanics* 5 (1) (2011) 55–66.
- [12] Seitzl, S., García, T. E., Fernández-Canteli, A., In- and out-of plane constraint effects on the fracture parameters of Aluminum alloy 2024: Finite element modeling and experimental results, *Proceedings of the 27th Conference on Computational Mechanics*, Plzen, Czech Republic, 2011.
- [13] Ševčík, M., Hutař, P., Zouhar, M., Náhlík, L., Numerical estimation of the fatigue crack front shape for a specimen with finite thickness, *International Journal of Fatigue* 39 (2012) 75–80.
- [14] She, Ch., Guo, W., The out-of-plane constraint of mixed-mode cracks in thin elastic plates, *International Journal of Solids and Structure* 44 (2007) 3 021–3 034.

- [15] Standard test method for measurement of fracture toughness, ASTM E1820-05, 2011.
- [16] Tada, H., Paris, P. C., Irwin, G. R., The stress analysis of cracks handbook (3rd ed.). American Society of Mechanical Engineers 2000.
- [17] Williams, M. L., On the stress distribution at the base of a stationary crack, Journal of Applied Mechanics 24 (1957) 109–114.